Available online at www.sciencedirect.com
ScienceDirect
Journal of Sound and Vibration 317 (2008) 841–865
JOURNAL OF SOUND AND VIBRATION
www.elsevier.com/locate/jsvi

Vibration response of a cracked rotor in presence of rotor–stator rub

Tejas H. Patel[a,b], Ashish K. Darpe[b,*]

[a]*Department of Mechanical Engineering, Charotar Institute of Technology, Changa 388421, India*
[b]*Department of Mechanical Engineering, Indian Institute of Technology, Delhi 110016, India*

Received 2 December 2007; received in revised form 13 March 2008; accepted 16 March 2008
Handling Editor: L.G. Tham
Available online 9 May 2008

Abstract

Fatigue crack and rotor–stator rub are two important faults in rotating machinery. Researchers have mostly studied the vibration behavior of a rotor with crack and rotor–stator rub separately. However, once the crack is developed in a rotor, the rotor is more likely to make contact with stator under tight clearance conditions, due to increased vibration level. The present study is aimed to examine vibration response of the cracked rotor in presence of common rotor faults such as unbalance and rotor stator rub. Numerical and experimental investigations are carried out and steady-state vibration analysis is presented. Experimental investigation for a multifault rotor system is attempted for the first time. The full spectrum analysis has been used effectively to extract the distinctive directional features of these rotor faults. The investigation focuses on directional nature of the higher harmonics for identification of rub in the cracked rotor. The study reveals that spectrum rich in spectral lines is a rub symptom. However, these higher harmonics are weaker than the 1X response. Rub in uncracked rotor excites forward and backward whirling frequency components almost equally. Cracked rotor without rub exhibits strongly forward whirling vibrations. Rotor rub in the cracked rotor reveals different response compared with the uncracked rotor, particularly the nature of 2X and higher harmonics at corresponding subharmonic resonances. Backward whirling nature of 2X frequency component as well as that of higher harmonic (that matches with the bending natural frequency) at corresponding subharmonic resonances, has been proposed for diagnosis of rotor rub in cracked rotor.

1. Introduction

An ever-increasing pursuit of higher power and efficiency has lead to highly stressed condition of rotating machine elements. Rotors are becoming more flexible and operating under tighter clearances and harsh environment. Under these circumstances, the rotors are likely to develop one or more faults, e.g. crack, rub, bow, etc. Fatigue cracking and rotor–stator rubbing are two important faults in rotating machines. Extensive reviews of the literature on vibration of cracked shaft are presented by Dimarogonas [1] and Sabnavis et al. [2]. It is well known from the past literature [3–5] that along with increase in 1X rev. component, rotor crack

*Corresponding author.
E-mail address: akdarpe@mech.iitd.ernet.in (A.K. Darpe).

0022-460X/$ - see front matter © 2008 Elsevier Ltd. All rights reserved.
doi:10.1016/j.jsv.2008.03.032

induces periodic steady-state lateral vibrations at twice and thrice the rotation speed (i.e. 2X and 3X rev. components) due to breathing of the crack under gravity loading. There has been extensive research on issues related to rotor–stator contact-related problems. Muszynska [6] presented excellent review of the rub-related issues. Beatty [7] used the elastic impact-contact model with Fourier-series expansion for the mathematically generated rotor response signal with rubbing condition. Ehrich [8] observed supercritical subharmonic response characterized by appearance of chaotic behavior in the transition zone between successive orders of subharmonic response. Feng and Zhange [9] discussed vibration response of a rotor rubbing caused by an initial perturbation. They discussed influence of various parameters on the vibration phenomena of the rotor system. Chu and Lu [10] observed very rich form of periodic and chaotic vibrations in their experimental study. They found that besides harmonic components 2X and 3X, the 1/2 fractional harmonic components such as 1/2X, 3/2X, etc., and the 1/3 fractional harmonic components such as 1/3X, 2/3X, etc., are also present in some of the cases.

It is common practice to address fault identification in isolation from all other disturbing mechanisms. Unbalance apart, most of past studies do not account for the presence of any other fault while investigating the vibrations related to cracked rotor or rotor rub. A typical rotor-bearing system may very often be a multifault system. For example, a rotor system can always has some amount of unbalance, misalignment in the drive line, temporary bow, etc. However, these can be within the permissible limits. Simultaneous existence of multiple faults is more realistic situation for the rotor system, particularly when the rotors are operating under severe thermal and mechanical stresses. In such situations, when more than one fault coexists in the rotor-bearing system, the problem of relating the observed vibration response to a particular fault could become a rather difficult task. In recent past, few research studies have addressed this issue.

Bachschmid et al. [11] applied model-based technique for multiple faults identification using least-square fitting approach by means of minimization of multidimensional residual between the vibrations in some measuring planes. They showed that the method effectively locates and sizes one or two simultaneous faults. For one fault, identification was nearly perfect, but, for two faults the error as low as 2% and as high as 66% were reported for some of the cases. Chan and Lai [12] analyzed four cases: (i) uncracked symmetrical shaft; (ii) cracked symmetrical shaft; (iii) uncracked asymmetrical shaft; and (iv) cracked asymmetrical shaft. They noticed that resonance at half of the critical speed in the responses of cracked shaft and asymmetric shaft. However, cracked shafts (cases (ii) and (iv)) also show resonance at one-third the critical speed which asymmetric uncracked shaft did not. At half the critical speed, higher levels of vibrations were observed for cracked asymmetrical shaft compared with the cracked symmetrical shaft. The levels of vibrations were even larger than that at critical speed. This feature has been suggested as a reliable indicator for detecting shaft cracks in symmetric rotors. Darpe et al. [13] studied dynamics of two crack rotor. They modelled one crack as breathing fatigue crack and other as open crack to simulate the rotor stiffness asymmetry. Through orbital plots and frequency spectra, different diagnostic features were proposed to distinguish stiffness asymmetry from crack. Darpe et al. [14] investigated the effect of bow on the nonlinear nature of the crack response. Reduction in amplitude of the response during cost up at self-balancing speed and presence of non-zero response amplitude at the self-balancing speed were, respectively, the proposed indicators for identification of cracked rotor and bowed rotor, when both crack and bow coexists. Wan et al. [15] have investigated vibration of a cracked rotor sliding-bearing system with rotor stator rubbing, using harmonic wavelet transform. Though they observed differences in wavelet time–frequency maps of cracked rotor with and without rubbing, they have not separated out the distinctive features related to crack and rubbing. These are few of the studies where two faults have been accounted in the rotor model apart from unbalance.

Fault identification in rotating machinery using vibration analysis is a constantly expanding field. With development in sensor technology, computing power and increase in knowledgebase; different signal processing techniques were evolved over a period of time. Spectral analysis using fast Fourier transform (FFT) algorithm is widely used technique for vibration analysis of the rotors because the spectral components and their amplitudes vary in accordance with various fault mechanisms. The conventional FFT treats vibration signal as real quantities so frequency spectrum looses important orbital information such as directivity i.e. forward or backward. Full spectrum overcomes this limitation by retaining the relative phase information between two measured vibration signals [16]. This attribute makes full spectrum one of the important

diagnostic tools. Lee and Han [17] used shape and directivity information of the instantaneous planar motion and its inclination to detect symptoms of the some types of the faults. Bachschmid et al. [18] demonstrated significance of the orbit shape analysis to improve machine fault detection. Fengui and Meng [19] presented the full spectrum cascade analysis of acceleration signal for some compound rub malfunctions. Based on full spectra of experimental acceleration signal, diagnostic features were studied.

The rotor to stator rubbing is considered as a secondary phenomenon resulting from primary cause, which perturbs the machine during normal operation. These primary causes could be rotor vibrations (due to unbalance, crack, or other energy sources) and/or displacements of rotor centreline, due to rotor misalignment, gravity force, fluid forces, etc. For the reasons cited above, it is important to examine the behavior of one fault mechanism in presence of other disturbing functions, because sometimes presence of one fault may lead to the generation of other fault, for example higher levels of vibration due to crack in rotor may develop rotor stator rubbing in tight clearance situation. Both these faults (crack and rub) introduce nonlinearity to the system of equations, generating higher harmonics in the response. In such situation, it is important to understand their specific vibration signatures for unique fault identification. Thus, the primary objective of the study is to investigate the vibration characteristics of cracked rotor in presence of unbalance and rotor–stator rub. However, the study is also made to identify unique vibration features of crack and rub faults in presence of unbalance. The equations of motion of the cracked Jeffcott rotor with unbalance and rotor–stator rub are presented. The steady-state vibration response is obtained in presence of rotor faults (i.e. unbalance, fatigue crack, and rotor–stator rub). The full spectrum analysis is applied to extract the distinctive directional feature of the rotor system when these rotor faults exist together. Results obtained from numerical simulations are verified by experimental work. Based on the study some diagnostic recommendations are derived.

2. Equations of motion of the cracked rotor with rub-impact

2.1. Equations of motion

A Jeffcott rotor is considered on rigid-bearing supports having a central disk of mass m on the shaft of length L. Transverse surface crack of depth a, is assumed at the mid span of the rotor. Fig. 1(a) shows the coordinates (Y and Z are the fixed coordinates and ξ and η are the rotating coordinates) in the crack cross-section. ξ is the weak crack direction and η is the strong crack direction. The unbalance eccentricity ε is assumed to be at an angle β with the weak crack direction. $\theta(t)$ is the instantaneous angle of rotation and ω is the rotor speed. The equations of motion for the cracked Jeffcott rotor, can be written in fixed coordinate Y–Z system (Fig. 1(a)) as

$$\begin{aligned} m\ddot{Y} + c\dot{Y} + k_y Y + k_{yz} Z &= F_y + m\varepsilon\omega^2 \cos(\theta + \beta) - mg, \\ m\ddot{Z} + c\dot{Z} + k_{zy} Y + k_z Z &= F_z + m\varepsilon\omega^2 \sin(\theta + \beta). \end{aligned} \tag{1}$$

The forces F_y and F_z are the nonlinear rub forces. k_y and k_z are direct and k_{yz} and k_{zy} are cross-stiffness coefficients of the cracked rotor, defined in the fixed coordinate system. These coefficients are calculated from the stiffness coefficients k_ξ, k_η, $k_{\xi\eta}$, and $k_{\eta\xi}$ defined in the rotational frame in a cross-section containing the transverse fatigue crack. In breathing crack model considered for present study, amount of open part of the crack continuously changes with shaft rotation, thereby accounting partial open/close state of the crack. Due to this partial opening and closing of the crack, cross-stiffness terms $k_{\xi\eta}$ and $k_{\eta\xi}$ appear in the equations of motion (Eq. (1), as $k_{\xi\eta}$ is related to k_{yz}). However, $k_{\xi\eta}$ comes out to be equal to the $k_{\eta\xi}$:

$$\begin{bmatrix} k_y & k_{yz} \\ k_{zy} & k_z \end{bmatrix} = T^{-1} \begin{bmatrix} k_\xi & k_{\xi\eta} \\ k_{\eta\xi} & k_\eta \end{bmatrix} T, \tag{2}$$

where the transformation matrix is

$$T = \begin{bmatrix} \cos\theta & \sin\theta \\ -\sin\theta & \cos\theta \end{bmatrix}.$$

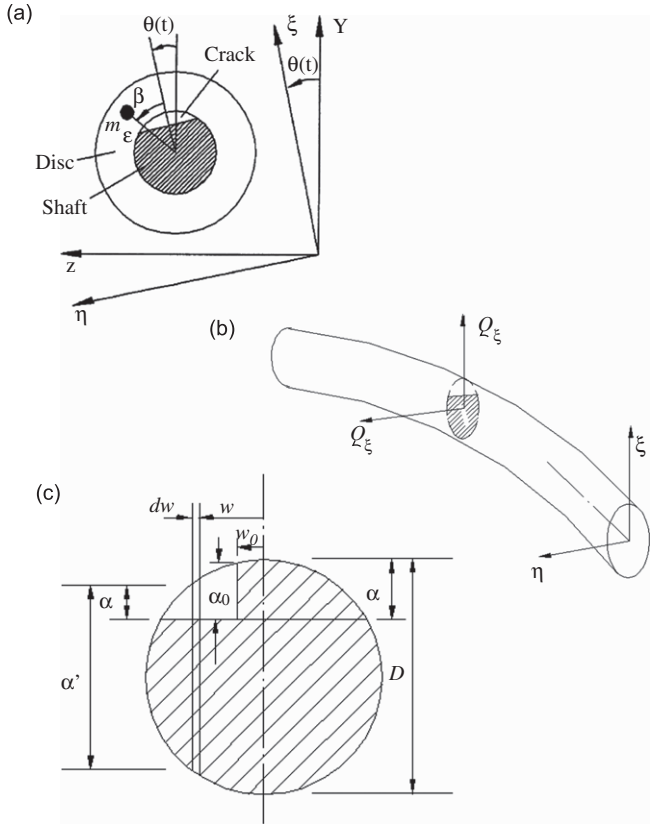

Fig. 1. (a) Coordinate system, (b) forces acting at the crack location, and (c) cross-section at crack location [14].

The equations of motion (Eq. (1)) can be rewritten as

$$\begin{aligned} &m\ddot{Y} + c\dot{Y} + \frac{1}{2}\{k_\xi + k_\eta + (k_\xi - k_\eta)\cos 2\theta - 2k_{\xi\eta} \sin 2\theta\} Y \\ &\quad + \frac{1}{2}\{(k_\xi - k_\eta)\sin 2\theta + 2k_{\xi\eta} \cos 2\theta\} Z = F_y + m\varepsilon\omega^2 \cos(\theta + \beta) - mg, \\ &m\ddot{Z} + c\dot{Z} + \frac{1}{2}\{k_\xi + k_\eta + (k_\eta - k_\xi)\cos 2\theta + 2k_{\xi\eta} \sin 2\theta\} Z \\ &\quad + \frac{1}{2}\{(k_\xi - k_\eta)\sin 2\theta + 2k_{\xi\eta} \cos 2\theta\} Y = F_z + m\varepsilon\omega^2 \sin(\theta + \beta). \end{aligned} \tag{3}$$

It should be noted that in case of uncracked rotor, $k_{\xi\eta}$ and $k_{\eta\xi}$ terms vanish and $k_\xi = k_\eta = k_0$. Here k_0 is the stiffness of uncracked shaft.

2.2. Calculation of stiffness coefficients of cracked rotor

Using linear elastic fracture mechanics theory, stiffness coefficients k_ξ, k_η, $k_{\xi\eta}$, and $k_{\eta\xi}$ are computed from flexibilities of the cracked shaft [3,14], as follows:

$$k_\xi = \frac{g_\eta}{g_\xi g_\eta - g_{\xi\eta}^2}, \quad k_\eta = \frac{g_\xi}{g_\xi g_\eta - g_{\xi\eta}^2}, \quad k_{\xi\eta} = k_{\eta\xi} = \frac{-g_{\xi\eta}}{g_\xi g_\eta - g_{\xi\eta}^2}. \tag{4}$$

where g_ξ and g_η are direct and $g_{\xi\eta}$ and $g_{\eta\xi}$ are cross-flexibilities of the cracked rotor. Total flexibility of the shaft made up of two parts: one is the flexibility of uncracked shaft and second is the additional flexibility introduced by the crack. The flexibility introduced by crack, changes with the amount of the open part of

crack. As the rotor rotates, the crack breathes. The amount of open part of the crack constantly changes, thereby changing the flexibility of the cracked rotor. In this way, partial opening and closing of the crack is accounted in the model. The flexibilities are computed using

$$g_\xi = \frac{L^3}{48EI} + \iint \frac{128L^2\alpha'^2\alpha}{E\pi D^8} F(\alpha/\alpha')^2 \,\mathrm{d}\alpha\,\mathrm{d}w,$$
$$g_\eta = \frac{L^3}{48EI} + \iint \frac{512L^2w^2\alpha}{E\pi D^8} F'(\alpha/\alpha')^2 \,\mathrm{d}\alpha\,\mathrm{d}w,$$
$$g_{\xi\eta} = g_{\eta\xi} = \iint \frac{256L^2\alpha'^2w}{E\pi D^8} \alpha F(\alpha/\alpha')F'(\alpha/\alpha') \,\mathrm{d}\alpha\,\mathrm{d}w. \tag{5}$$

where functions F and F' in Eq. (5) are given by [20],

$$F(\alpha/\alpha') = \sqrt{\frac{2\alpha'}{\pi\alpha}\tan\left(\frac{\pi\alpha}{2\alpha'}\right)}\,\frac{0.923 + 0.199[1-\sin(\pi\alpha/2\alpha')]^4}{\cos(\pi\alpha/2\alpha')}. \tag{6}$$

$$F'(\alpha/\alpha') = \sqrt{\frac{2\alpha'}{\pi\alpha}\tan\left(\frac{\pi\alpha}{2\alpha'}\right)}\,\frac{0.752 + 2.02(\alpha/\alpha') + 0.37[1-\sin(\pi\alpha/2\alpha')]^3}{\cos(\pi\alpha/2\alpha')}. \tag{7}$$

The term $L^3/48EI$ in Eq. (5) represents the flexibility of the uncracked shaft. It is important to note that, integration limits in expressions of Eq. (5) are from 0 to α for depth of crack and the limits for width are not specified. The limits of integration on width depend on the open part of the crack, which can be obtained from the sign of SIF (Eq. (8)) along the crack edge. After finding the total SIF, K^I (i.e. opening mode) at various locations on crack edge, the position where SIF changes the sign can be found out. The positive SIF indicates the tensile stress field and the crack in open state, whereas, negative SIF indicates compressive stress field and the crack in close state. Once the amount of open part is known, integration can be performed for the open part of the crack:

$$K^I = \sigma_\xi\sqrt{\pi\alpha}F(\alpha/\alpha') + \sigma_\eta\sqrt{\pi\alpha}F'(\alpha/\alpha'), \tag{8}$$

where σ_ξ and σ_η are the bending stresses due to Q_ξ and Q_η, respectively (Fig. 1(b)). They are given by

$$\sigma_\xi(w) = \frac{(Q_\xi L/4)(\alpha'/2)}{I}, \quad \sigma_\eta(w) = \frac{(Q_\eta L/4)w}{I}, \tag{9}$$

where $I = \pi D^4/64$, $\alpha' = \sqrt{D^2-(2w)^2}$, and

$$Q_\xi = k_\xi\xi + k_{\xi\eta}\eta, \quad Q_\eta = k_{\eta\xi}\xi + k_\eta\eta. \tag{10}$$

There are numerous crack breathing models available in the literature. Earlier studies on vibration response of the cracked rotor mostly considered bi-level stiffness model where the rotor assumed to possess bi-levels of rotor stiffness corresponding to closed and open state of the crack. Several researchers then realised that in all actual rotors, opening/closing of the crack is likely to be gradual and modelled the crack breathing with assumption of sinusoidal stiffness variation (for example, Refs. [4,21]). However, the boundary between opened and closed part of the crack varies continuously with shaft rotation depending upon the forces acting at the crack section. Thus, the stiffness variation as a function of rotor orientation only may not be appropriate in certain situations particularly for unsteady and transient loading on the shaft. The present work considers this aspect and models the transverse fatigue crack with variable open–close area of crack, where, the sign of total intensity factor K^I (Eq. (8)) is used to decide the open/close part of the crack. The crack stiffness estimation thus adapts to variety of rotor loadings and forces.

2.3. Rub-impact forces

Forces F_y and F_z in Eq. (2), are the nonlinear rub forces generated from the interactions between the rotor and stator. Rotor rubbing impacts may occur intermittently and could be for very short duration. The rotor is assumed to impact elastically with hard stator. Coulomb-type frictional relationship is considered at the

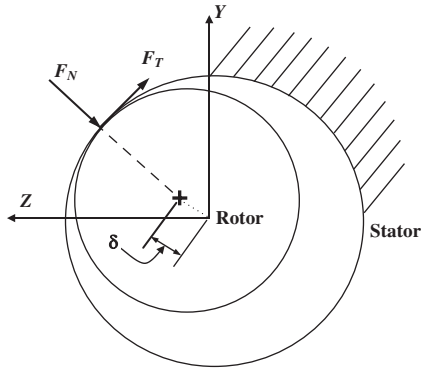

Fig. 2. Rotor stator rub-impact.

contact. When rub occurs as shown in Fig. 2, the radial impact force F_N and tangential rub force F_T can thus be expressed as [7]

$$F_N = \begin{cases} 0 & \text{for } (e<\delta) \\ (e-\delta)k_s & \text{for } (e\geqslant\delta) \end{cases} \quad \text{and} \quad F_T = \mu F_N, \tag{11}$$

where $e = \sqrt{Y^2+Z^2}$ is the radial displacement of the rotor, δ the clearance between rotor and stator, μ the coefficient of friction, and k_s the stator stiffness. The forces F_y and F_z can be written as

$$F_y = -F_N\left(\frac{Y}{e}\right) - \psi_f F_T\left(\frac{Z}{e}\right), \quad F_z = -F_N\left(\frac{Z}{e}\right) + \psi_f F_T\left(\frac{Y}{e}\right) \quad \text{or}$$

$$\begin{Bmatrix} F_y \\ F_z \end{Bmatrix} = -\frac{(e-\delta)k_s}{e}\begin{bmatrix} 1 & \psi_f\mu \\ -\psi_f\mu & 1 \end{bmatrix}\begin{Bmatrix} Y \\ Z \end{Bmatrix} \quad \text{for } e\geqslant\delta \quad \text{and}$$

$$\begin{Bmatrix} F_y \\ F_z \end{Bmatrix} = \begin{Bmatrix} 0 \\ 0 \end{Bmatrix} \quad \text{for } e<\delta, \tag{12}$$

where ψ_f is the function, to decide the direction of frictional forces

$$\psi_f = \begin{cases} -1 & \text{for } \omega R + v_t > 0, \\ 0 & \text{for } \omega R + v_t = 0 \\ 1 & \text{for } \omega R + v_t < 0. \end{cases} \quad \text{and} \quad v_t = \dot{Z}\left(\frac{Y}{e}\right) - \dot{Y}\left(\frac{Z}{e}\right), \tag{13}$$

Solution to the nonlinear nonautonomous equations of motion (Eq. (3)) is obtained using Runge–Kutta fourth-order numerical integration scheme. A small time step is chosen in order to ensure a stable solution and to avoid the numerical divergence at the point where derivatives of F_y and F_z are discontinuous. Long-time marching technique is adopted to obtain stabilized steady-state response. It should be noted that Eq. (3) are generalized equations of motion for rotor–stator rub in cracked rotor. However, with little modifications in equations of motion, vibration response can also be obtained for the cases of uncracked rotor without rub, cracked rotor without rub and uncracked rotor with rub. For the uncracked rotor, $k_{\xi\eta}$ and $k_{\eta\xi}$ terms vanish in Eq. (3) and $k_\xi = k_\eta = k_0$. Where k_0 is stiffness of uncracked shaft. To study rotor response without rotor rub, the forces F_y and F_z are set to zero in Eq. (3).

3. Full spectrum analysis of vibration signal

The full spectrum is based on the rotor vibration data from lateral directions (i.e. Y and Z). In other words, it is the spectrum of an orbit [16]. At a glance, the full spectrum plot tells us whether the rotor orbit frequency components are forward or backward in whirl, in relation to the rotor spin direction.

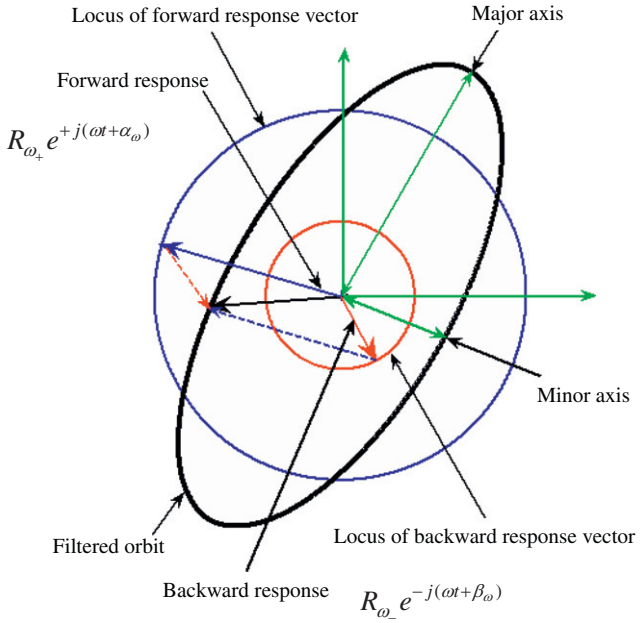

Fig. 3. Decomposition of elliptical orbit in to forward and backward whirling orbits [16].

The process of computing either full or half-spectrum starts form digitizing the vibration waveforms. In case of Y–Z probes measuring the rotor vibration, there is one waveform from each channel. Combined they generate a direct orbit. Half-spectrums are independently calculated from each waveform. During this calculation, a part of the information contained in the waveform, in particular, the relative phase correlation between Y and Z spectrum components is not displayed. Full spectrum overcomes this limitation by retaining the directional information of each frequency components. The process of obtaining a full spectrum includes an expansion of the direct orbit in to a sum of filtered orbits. Each filtered orbit has, in general, an elliptical shape. An elliptical orbit can be presented as a sum of two circular orbits: one is the locus of vector rotating in the direction of rotation (i.e. forward whirling component), and the other is the locus of vector rotating in opposite direction (i.e. reverse whirling component). Fig. 3 is the vectorial representation of the same.

Using the complex notations, let the harmonic signal be represented by $p(t)$, having frequency ω. The real and imaginary parts of the complex signal $p(t)$ are the real vibration signals, in two orthogonal directions Y and Z, respectively. Therefore, the signal $p(t)$ in polar form can be written using Euler's formula as

$$p(t) = y(t) + jz(t) = p_{\omega_+}(t) + p_{\omega_-}(t) = R_{\omega_+}\mathrm{e}^{\mathrm{j}(\omega t+\alpha_\omega)} + R_{\omega_-}\mathrm{e}^{-\mathrm{j}(\omega t+\beta_\omega)}, \tag{14}$$

$$p(t) = \tfrac{1}{2}\{(y_d + z_q) + j(z_d - y_q)\}\mathrm{e}^{\mathrm{j}\omega t} + \tfrac{1}{2}\{(y_d - z_q) + j(z_d + y_q)\}\mathrm{e}^{-\mathrm{j}\omega t}, \tag{15}$$

where

$$\begin{gathered} p_{\omega_+}(t) = R_{\omega_+}\mathrm{e}^{\mathrm{j}(\omega t+\alpha_\omega)}, \quad p_{\omega_-}(t) = R_{\omega_-}\mathrm{e}^{-\mathrm{j}(\omega t+\beta_\omega)}, \\ y(t) = y_d \cos\omega t + y_q \sin\omega t, \quad z(t) = z_d \cos\omega t + z_q \sin\omega t, \\ R_{\omega_+} = \tfrac{1}{2}\sqrt{(y_d + z_q)^2 + (z_d - y_q)^2}, \quad R_{\omega_-} = \tfrac{1}{2}\sqrt{(y_d - z_q)^2 + (z_d + y_q)^2}. \end{gathered} \tag{16}$$

Here, R_{ω_+} and R_{ω_-} are the radii of the forward and reverse orbits, ω is the frequency of filtering, α_ω and β_ω are phases of forward and reverse responses, and y_d, y_q, z_d and z_q are the direct and quadrature parts of the filtered signals $y(t)$ and $z(t)$, respectively.

The $p(t)$ represents the instantaneous position of the rotor on the forward and reverse filtered orbits. Note that the major axis of the filtered orbit is $R_{\omega_+} + R_{\omega_-}$, while its minor axis is $|R_{\omega_+} - R_{\omega_-}|$. Forward precession

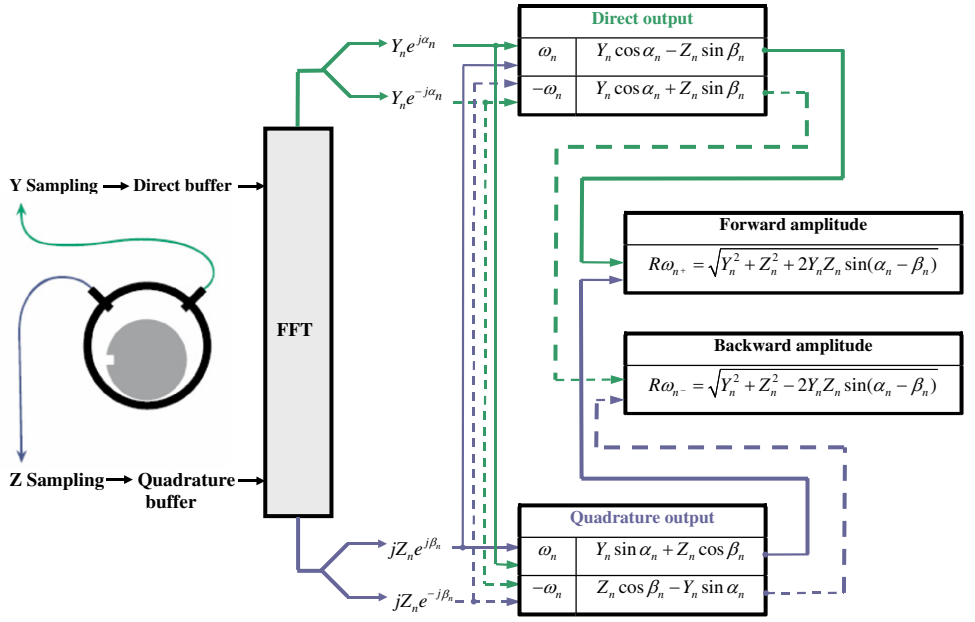

Fig. 4. Mathematical procedure for obtaining a full spectrum [16].

of the filtered elliptical orbit (in the direction of the rotor rotation) means that, $R_{\omega_+} > R_{\omega_-}$, while reverse precession (in opposite direction of rotor rotation) means that, $R_{\omega_+} < R_{\omega_-}$. The angle between the Y probe and the ellipse major axis, $(\beta_\omega - \alpha_\omega)/2$, is determined by the relative phase of forward and reverse components. The full spectrum can be constructed from the radii of forward and reverse components of the filtered orbits.

The procedure for obtaining the full spectrum from the half-spectrums of YZ probes is shown in Fig. 4 [16]. Simultaneously sampled Y and Z transducers data are put into the direct and quadrature part of the FFT input, respectively, consequently, the positive and negative frequency halves of the FFT are not the mirror images. The results are then subjected to another transform for Y to Z and for Z to Y precession. In right half part, the full spectrum plot presents the amplitude of the forward whirling frequency components (also known as positive frequency components) of signal. The left half part shows backward whirling frequency components (also known as negative frequency components) of the signal. It is important to note that the forward and reverse component amplitudes can be used to recover shape of the corresponding filtered orbit.

4. Numerical results and discussion

Values of the system parameter used for the numerical simulations are as follow: mass of the disk, $m = 6$ kg; shaft diameter, $D = 25$ mm; shaft length, $L = 0.7$ m; external damping, $c = 182.56$ N s/m; stator stiffness, $k_s = 140 \times 10^{+6}$ N/m; coefficient of friction, $\mu = 0.2$ and unbalance eccentricity, $\varepsilon = 1.0597 \times 10^{-5}$ m. Bending natural frequency of the rotor is 48.42 Hz. In this section, nonlinear response of the rotor–stator rub impact is analyzed for uncracked and cracked rotors. Results for cases without rotor rub are discussed first, and then for the cases with rub. The results are compared with derive useful diagnostic information.

4.1. Unbalance vibration response of uncracked and cracked rotors without rub

This subsection discusses the directional nature of the vibration response of the uncracked and cracked rotors in absence of rotor rub. Later on, this will be used to identify directional nature of the rotor response, when rub and crack coexist. Fig. 5 shows the full spectrum plots of unbalance vibration response of the uncracked rotor for the speed ratio, $p = 1/3$ and $1/2$ (where, $p = \omega/\omega_{cr}$), i.e. $1/3$ and $1/2$ of the bending natural frequency of the uncracked rotor. Amplitude of forward and backward whirling frequency components are calculated using the algorithm shown in Fig. 4 and plotted along $+$ve and $-$ve frequency axis to get the full

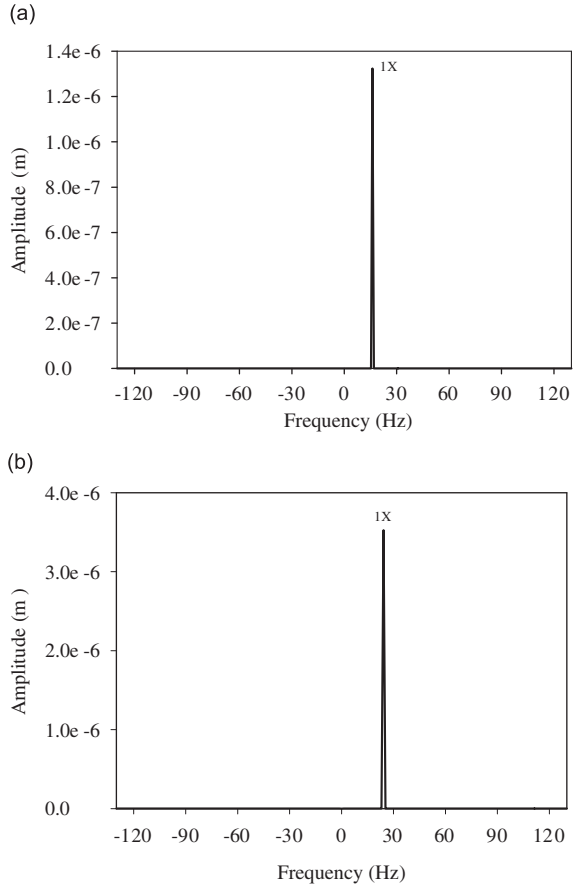

Fig. 5. Full spectrum plot of uncracked rotor without rub (a) $p = 1/3$ and (b) $p = 1/2$.

spectrum plot. Results indicate presence of synchronous frequency component along positive frequency axis only, i.e. backward whirling frequency component is not present. This highlights the well-known fact that unbalance excitation is synchronous with shaft rotation speed and the response due to unbalance is only forward whirling.

The crack due to the stiffness nonlinearity introduced because of breathing of crack shows the presence of strong harmonics in the response. Fig. 6 shows vertical vibration response, its FFT (i.e. single-sided spectrum) and full spectrum plot (i.e. double-sided spectrum) of vibration response of the cracked rotor ($a/D = 0.15$) for speed ratio, $p = 1/5$. It can be seen that the conventional frequency spectrum (Fig. 6(b)) shows the frequency components and its magnitude. On the other hand, full spectrum (Fig. 6(c)) clearly distinguish $+$ve frequencies from $-$ve frequencies of the vibration response and thus reveal the directional nature of vibrations. Vertical vibration signals and full spectra for $p = 1/3$ and $1/2$ are given in Fig. 7. It is observed that compared with uncracked rotor (Fig. 5), 1X response increases due to presence of crack. Synchronous vibration response at rotational speed i.e. 1X is forward (i.e. $+$ve) in nature, however, a weak backward (i.e. $-$ve) whirling 1X frequency component also appears in the spectra. Presence of this weak backward 1X frequency component along with the strong forward 1X frequency component is due to crack only, since uncracked rotor shows only $+1$X frequency components in full spectra (Fig. 5). Weak -2X, -3X, and -5X frequency components appear in spectra and vibration motion is forward whirling at these frequencies, as shown in full spectra of Figs. 6 and 7. Further, among -1X, -2X, -3X, and -5X frequencies, -2X frequency component is negligible, which suggests strongly forward whirling nature of the 2X harmonic for the cracked rotor. It is worth mentioning here that though the full spectrum plot is spectrum of orbit, it brings out the additional information about magnitude of different frequencies and more importantly the directional nature

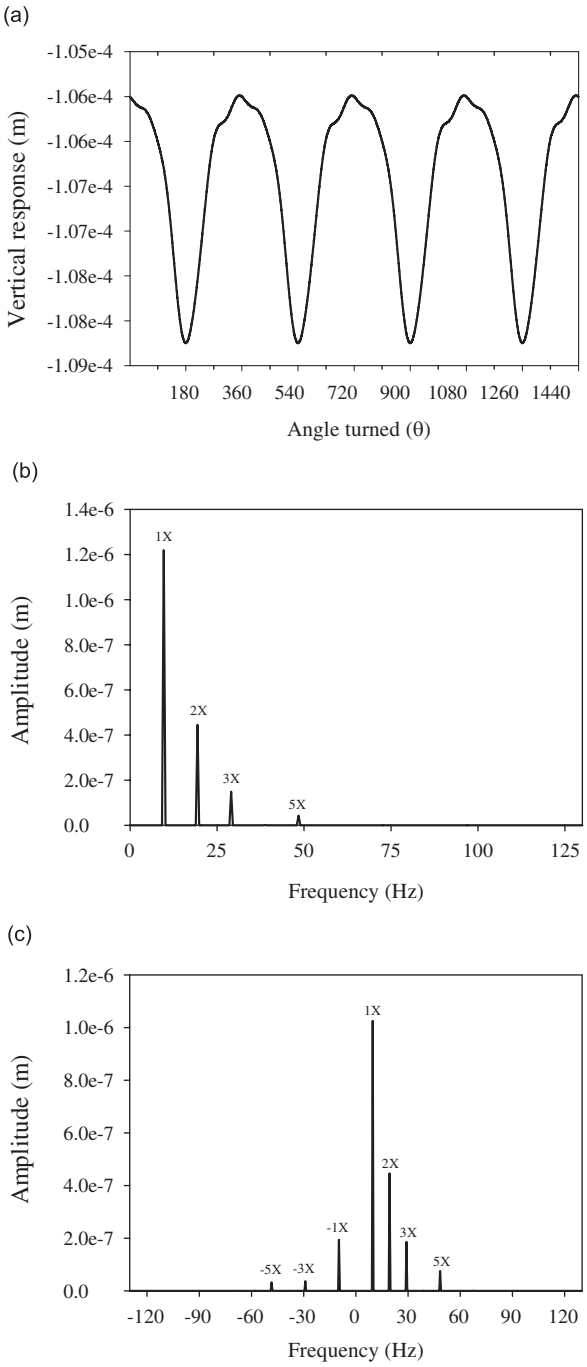

Fig. 6. Vibration response of cracked rotor ($a/D = 0.15$) without rub, $p = 1/5$: (a) vertical vibration response; (b) FFT; and (c) full spectrum.

of each of the frequency component. For example, orbit plots of Fig. 8, drawn for $p = 1/3$ and $1/2$ cannot reveal the directional nature of the vibrations at different spectral components, which was quite apparent from their full spectra (refer Fig. 7(i) and (ii)). With increase in crack depth (refer Fig. 9) increase in vibration levels is observed. From comparison of full spectra of cracked rotor with crack depths, $a/D = 0.28$ and 0.15, it may be noted that, 2X response becomes stronger in comparison with the 3X response, with increase in crack

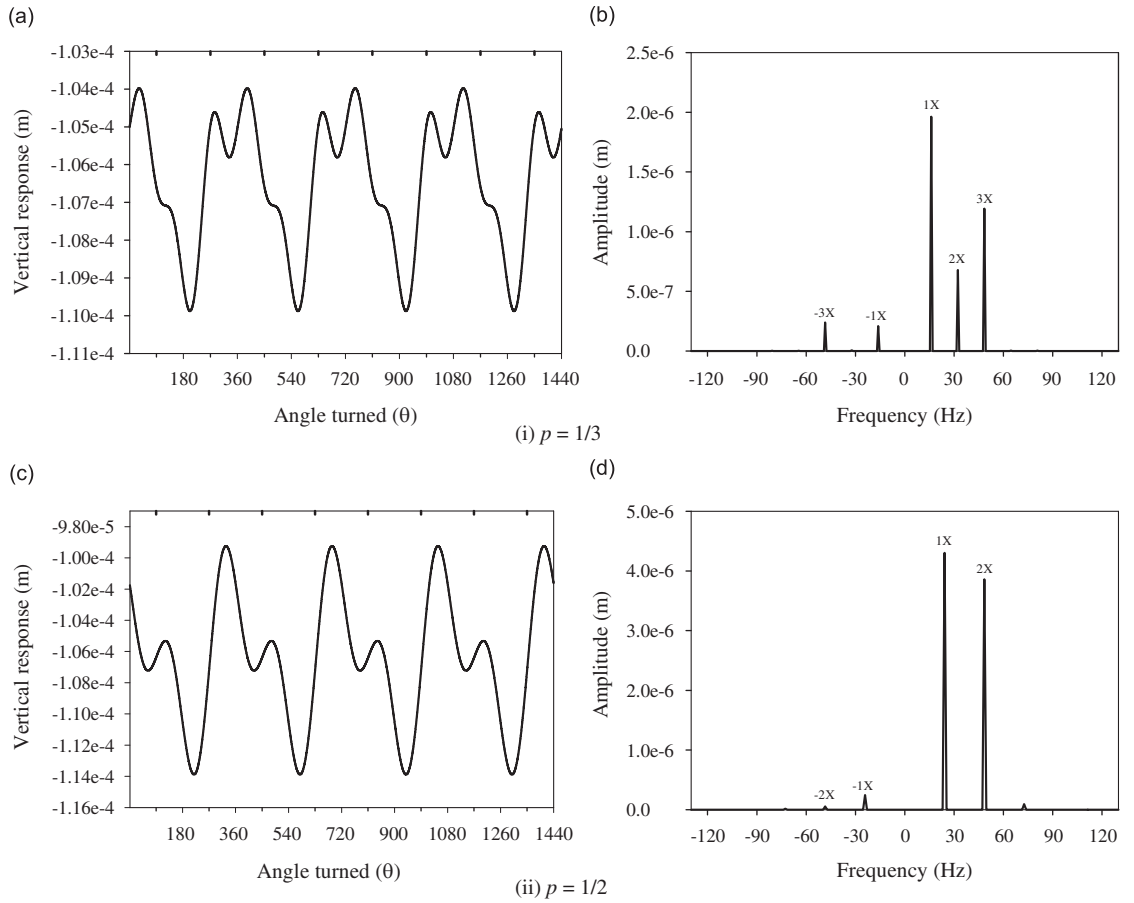

Fig. 7. Vibration response and full spectrum plots of cracked rotor ($a/D = 0.15$) without rub: (a, c) vertical vibration response; (b, d) full spectra; (i) $p = 1/3$ and (ii) $p = 1/2$.

depth. It may be noted that, in rotors with deeper cracks, the effect of increased stiffness asymmetry dominates the response compared with increased flexibility due to breathing behavior of crack. As a result, 2X vibration amplitude grows significantly in comparison to amplitude of 3X frequency component. From Figs. 6, 7, and 9, it is clear that the backward whirling 2X component is important parameter for diagnosis of crack. The other higher harmonic components (3X, 5X, etc.) show noticeable amplitude of backward whirling component in contrast to almost zero backward whirling 2X frequency amplitude.

4.2. Unbalance vibration response of uncracked and cracked rotors with rub

In literature [6,8,10], a variety of rub conditions were examined and subharmonic, super-harmonic, chaos, quasi-periodic and subsynchronous response were reported for rotor rub. Rotor comes in contact with stator when radial displacement increases beyond the clearance between rotor–stator, hence the rotor interacts with stator during a small portion of the cycle time. This corresponds to the introduction of a wideband excitation to the system and the complicated transient responses are thus caused in the system.

Rotor rub with stator are likely to be transient phenomena. Rub disappears as soon as clearance between rotor and stator increases beyond the total excursion of the rotor, due to wearing of the material from rotor and/or stator. However, this is not the case always. It is reported [6] that the rub, once initiated may persist and then develop into the full rubbing steady-state scenario.

During rotor stator contact, forces acting on the rotor are in normal and tangential directions to the contacting surfaces. The tangential force is due to friction between the meeting surfaces, which tries to

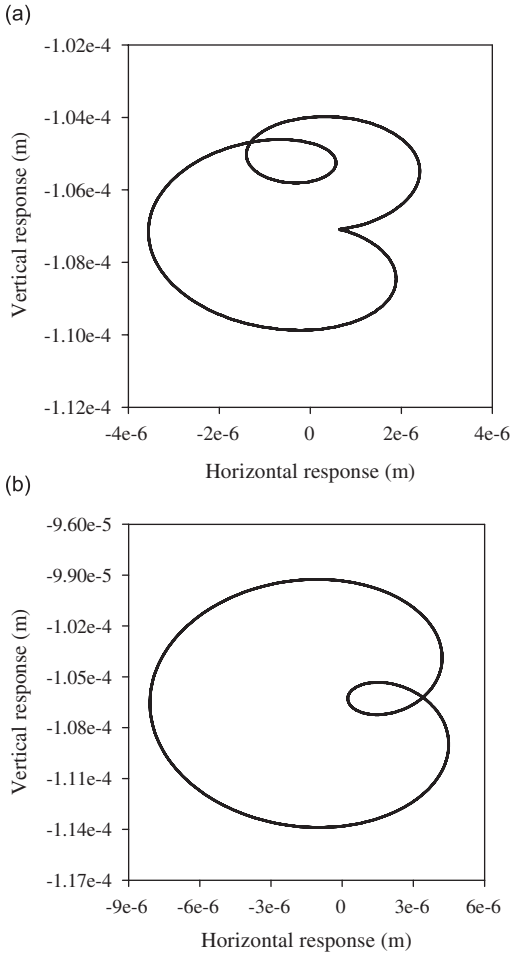

Fig. 8. Orbit plots of cracked rotor ($a/D = 0.15$) without rub: (a) $p = 1/3$ and (b) $p = 1/2$.

accelerate the rotor centerline in reverse precession direction. For this reason, rub produces reverse components in the full spectrum plots. In this subsection, influence of the rotor rub on the directional nature of the rotor vibrations are investigated for uncracked and cracked rotors. Rotor–stator clearance of 1.066×10^4 m is considered to simulate nonlinear rubbing effects. Results are first discussed for rotor rub in uncracked rotor and then for cracked rotor.

Fig. 10 shows the vertical vibration response its FFT and full spectra of the uncracked rotor with rub for $p = 1/3$ and $1/2$. For the given value of the rotor stator clearance, rub does not take place at $p = 1/5$. FFT plots indicate strong 1X motion, in presence of other spectral components. Though the spectrum is rich in harmonics, due to nonlinear rotor stator interactions, the harmonics are weaker in comparison with 1X frequency component. Both $+$ve and $-$ve higher harmonics are present in the full spectra. 1X frequency component is strongly forward whirling. It can be noted that the higher harmonics appear to be almost equal in magnitude. However, they are forward whirling, since the $+$ve frequencies are marginally stronger than the corresponding $-$ve frequencies, but sometimes the difference between $+$ve and $-$ve frequency amplitudes are very less (e.g. at $p = 1/3$ in this case) and hence difficult to notice such distinction. Full spectrum rich in harmonics with almost equal $+$ve and $-$ve frequencies is recommended as a rub signature. This feature is not observed for the cases of uncracked rotor and cracked rotor without rub (Figs. 5, 7, and 9), discussed earlier. Subharmonic resonances at $1/3$ and $1/2$ of the bending critical speed are not observed in for rubbing rotors. It should be noted that the directional information extracted by the full spectra, are missing in the FFT plots.

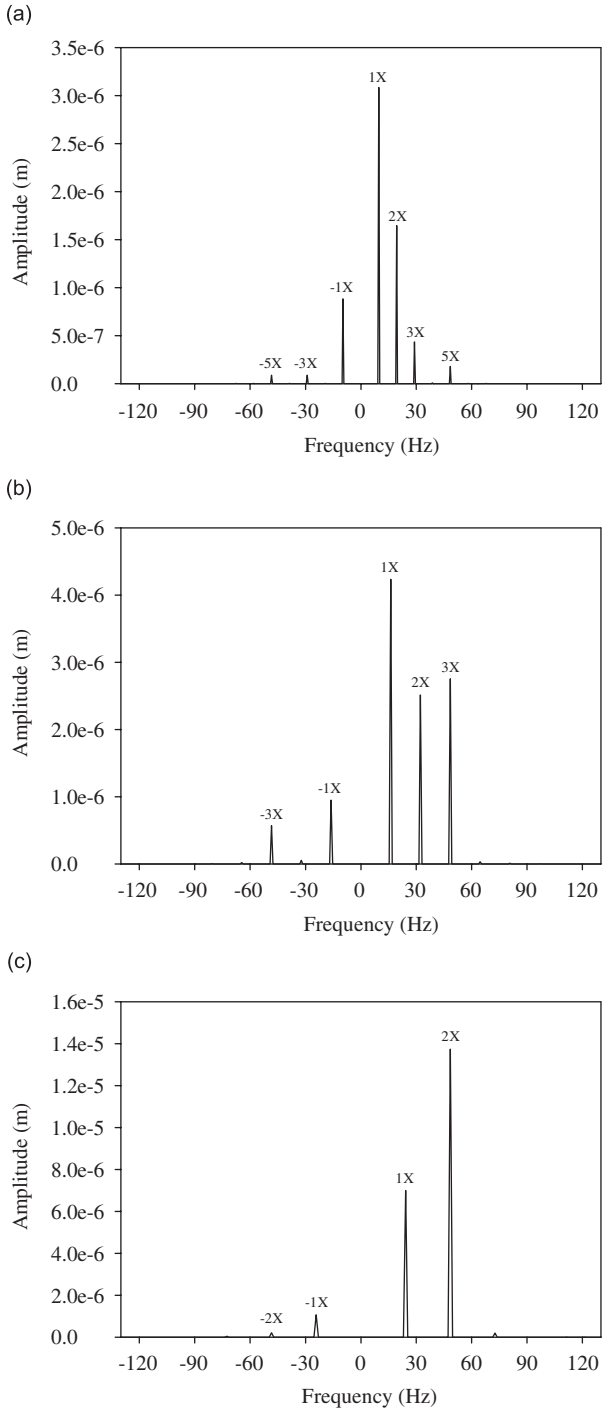

Fig. 9. Full spectrum plots of cracked rotor ($a/D = 0.28$) without rub: (a) $p = 1/5$, (b) $p = 1/3$, and (c) $p = 1/2$.

The foregoing simulations are carried out at fraction of bending critical speed. It may be mentioned that the choice of specific rotational speeds is not the prerequisite for the case of rub fault. Rotor–stator rub is highly nonlinear in nature and can exhibit chaotic, quasi-periodic, subharmonic, or super harmonic vibration response. Depending on the rotor–stator physical parameters and system parameters (such as rotation speed),

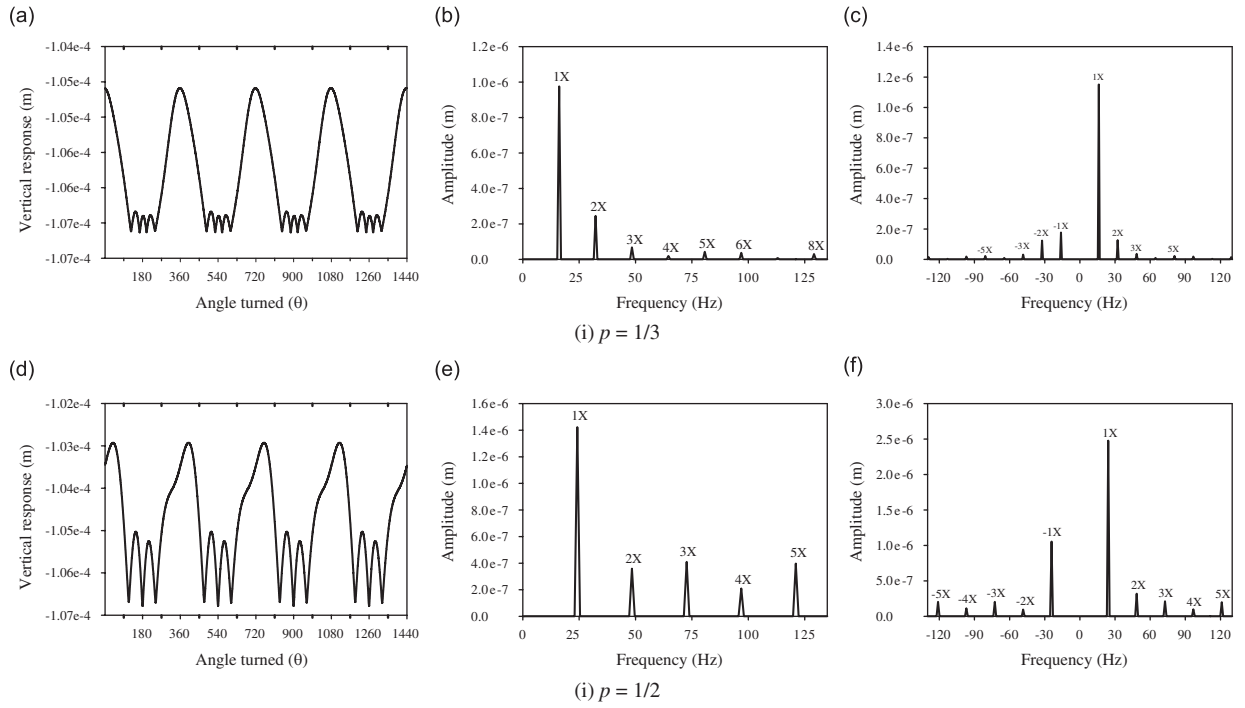

Fig. 10. Vibration response, FFT and full spectrum plots of uncracked rotor with rub; (a, d) vertical vibration response; (b, e) FFT; (c, f) full spectra; (i) $p = 1/3$ and (ii) $p = 1/2$.

the rub in rotor exhibits one or more of the above-mentioned vibration symptoms. On the other hand, the cracked rotor response reveals subharmonic resonances if operated at integer fraction of the critical speed (particularly at 1/5, 1/3, and 1/2 of the bending natural frequency) due to presence of higher harmonics in the vibration response. Hence, selection of rotor speeds at integer fraction of the critical speeds would clearly show up the typical crack vibration signatures. Thus, the idea here is to operate the rotor at integer fractions of bending critical speed and to understand differences in the response of crack and rub when they exist individually and when both exist together.

The breathing of the crack is governed by the gravity effect. Under the action of gravity force, crack opens and closes gradually in one rotation of the shaft. However, in presence of rubbing in cracked rotor, the combined effect of the rubbing forces, unbalance forces, and gravity determines the breathing of the crack, and in turn the vibration response of rub-impacting cracked rotors. To investigate the dynamics involved in rotor–stator interactions in cracked rotor, different crack depth ratios, $a/D = 0.15$, 0.28, and 0.4 are used for the simulations, to include the cases with shallow to deep cracks. Rest of the rotor parameters are same as mentioned earlier.

Fig. 11 shows the time-domain response in vertical direction, single-sided spectrum (FFT) and full spectrum plots, for the cracked rotor ($a/D = 0.15$) with rub for speed ratio $p = 1/5$. It should be noted that the 2X, 3X, and 5X harmonics are mainly due to crack and harmonics at 4X, 6X, etc. arise due to rub. These harmonics are clearly seen in FFT as well as full spectrum, but the full spectrum additionally reveals the whirl nature of this frequencies. Fig. 12 shows vertical vibration response and full spectra when $p = 1/3$ and 1/2. Vibration features specific to a cracked rotor, i.e. presence of strong 5X, 3X, and 2X frequency components at respective subharmonic resonance speeds (i.e. $p = 1/5$, 1/3, and 1/2), are clearly visible in full spectra. Typical rotor-rub indicator, i.e. spectrum rich in spectral lines, is also observed in the full spectra. Vibration response shows that, rotor rub modifies the vibration response of the cracked rotor. Comparing full spectra of vibration responses of uncracked and cracked ($a/D = 0.15$) rotors without rub (Figs. 5–7, respectively) and those with rub (Figs. 10–12, respectively), differences of nature of the vibrations is apparent. It should be noted that the rub was not observed for uncracked rotor at $p = 1/5$, however, due to presence of crack, the vibration level

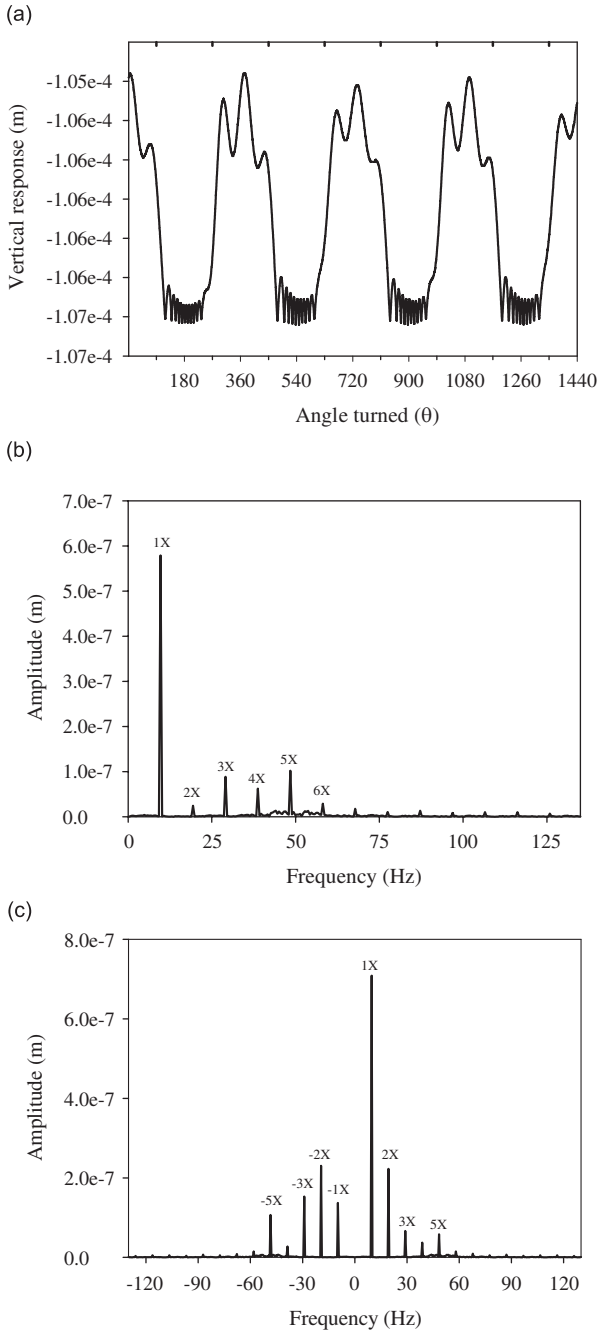

Fig. 11. Vibration response of cracked rotor ($a/D = 0.15$) with rub, $p = 1/5$: (a) vertical vibration response; (b) FFT; and (c) full spectrum.

increases slightly at $p = 1/5$, which is sufficient to develop rub in the cracked rotor. One important observation can be made regarding the nature of the twice the rotational frequency component (2X). In case of cracked rotor, the motion at 2X frequency is strongly forward with almost zero amplitude of backward whirl component. Harmonic at 2X frequency is weak for rub-impact in uncracked rotor in comparison with 1X. Though the difference between forward and backward whirling 2X components is very less and whirl at 2X harmonic is marginally forward. Whereas, in presence of both the rotor faults i.e. rub in cracked rotor, relatively strong backward 2X precession vibration motion is observed for all speed ratios $p = 1/5$, $1/3$, and

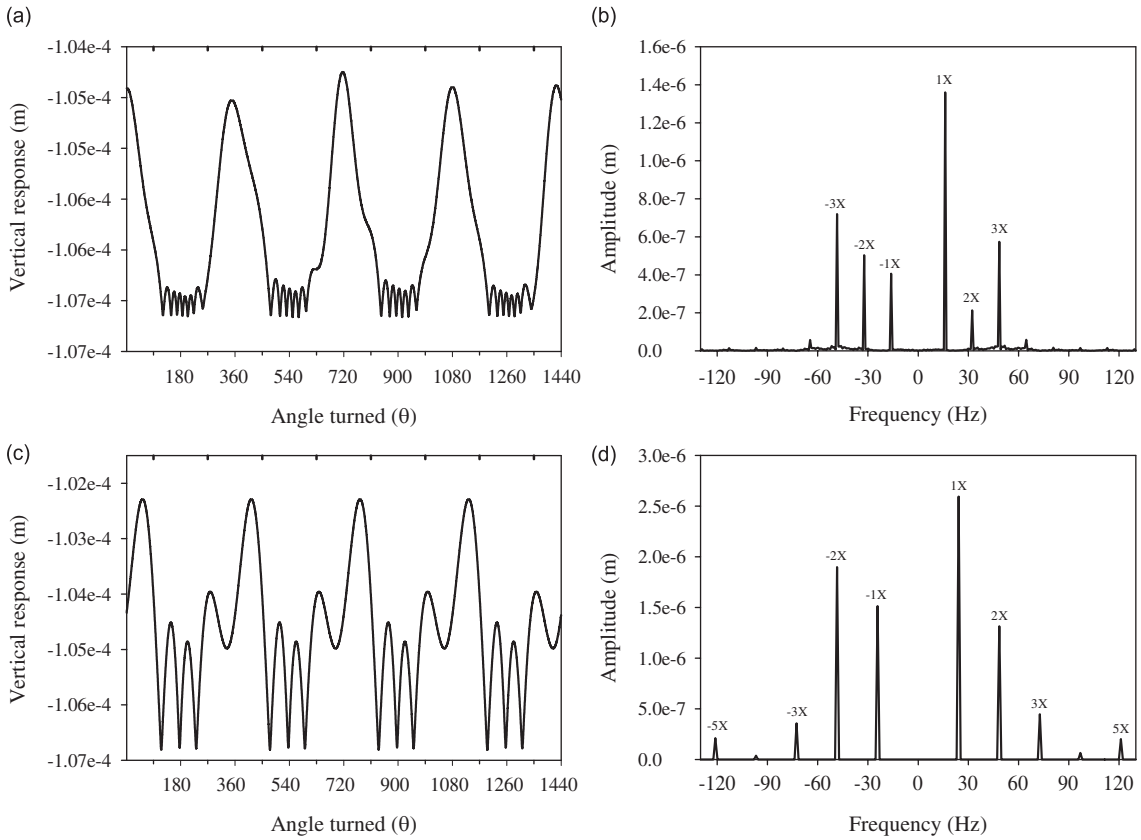

Fig. 12. Vibration response and full spectrum plots of cracked rotor ($a/D = 0.15$) with rub: (a, c) vertical vibration response; (b, d) full spectra; (i) $p = 1/3$ and (ii) $p = 1/2$.

1/2 (Figs. 11 and 12). This typical feature is quite noticeable particularly for the rotation speeds up to half the bending critical speed. Vibrations at 3X and 5X frequency components are backward whirling for $p = 1/3$ and 1/5, respectively. However, this trend of 3X and 5X harmonics is not regular, e.g. at $p = 1/2$, 3X response is forward whirling, although with a strong backward whirl component.

To understand more about the nature of motion at 3X and 5X frequency component and about the sensitivity of rotor response to crack depths, full spectrum plots of the vibration response of the cracked rotor for crack depths, $a/D = 0.28$ and $a/D = 0.4$ are obtained as shown in Figs. 13 and 14, respectively. The typical directional nature of the vibrations at 2X, 3X, and 5X frequency components noticed for crack depth $a/D = 0.15$, is also clearly noticed for higher crack depths, i.e. $a/D = 0.28$ and 0.4 with increased vibration amplitudes showing sensitivity of these fault detection parameters to the depth of crack. It should be noted that at $p = 1/5$ and 1/3, the 5X and 3X harmonics, respectively, matches with the bending natural frequency of rotor and the cracked rotor experience resonances at these speeds. Therefore, the vibrations of 3X and 5X frequency components are backward whirling, if they are excited due to corresponding subharmonic resonances (i.e. $p = 1/3$ or 1/5). Presence of strong 2X harmonic as well as 3X and 5X frequency components at respective subharmonic resonances is typical of cracked rotor and backward whirling nature of vibrations at these harmonics is attributed to the rub phenomena. It is important to emphasis here that when $p = 1/5$, rub has just initiated in the cracked rotor and vibration response still exhibits backward whirl for 2X and 5X harmonics. This signifies the effectiveness of these fault features even when the rub has just started developing.

It is important to recapitulate that, for rub in uncracked rotor, +ve and −ve higher harmonics are weaker compared with 1X and they are more or less equal in magnitude. In case of rub in cracked rotor, 2X, 3X, and 5X frequency components are sufficiently strong along both sides of full spectra. Hence, from diagnostics

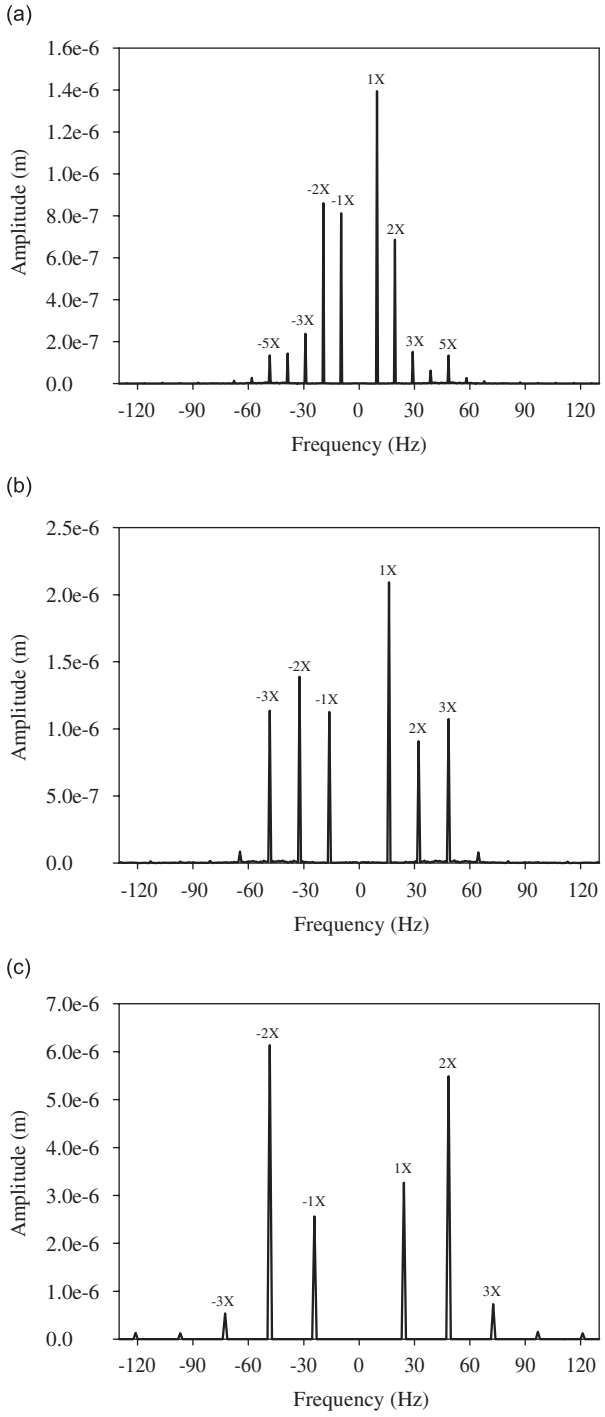

Fig. 13. Full spectrum plots of cracked rotor ($a/D = 0.28$) with rub: (a) $p = 1/5$, (b) $p = 1/3$, and (c) $p = 1/2$.

point of view, it is important to monitor the nature of motion of 2X frequency as well as higher harmonics at corresponding subharmonic resonances (i.e. 3X at $p = 1/3$ and 5X at $p = 1/5$). When rub occurs in cracked rotor, 2X vibration motion is backward in nature. Motion of 3X and 5X frequencies are backward whirling, when excited at subharmonic resonances at one-third and one-fifth of the critical speed, respectively. It may be noticed that this trend is consistently observed for all fractional critical speeds and crack depths considered for the study.

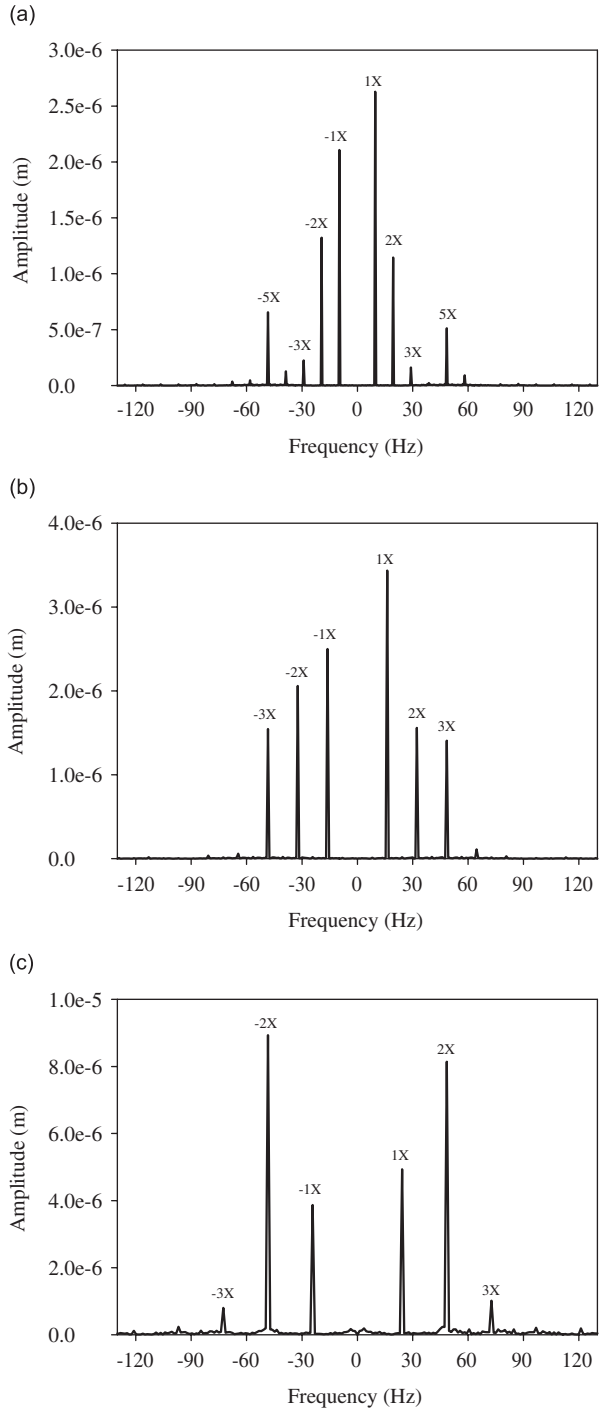

Fig. 14. Full spectrum plots of cracked rotor ($a/D = 0.40$) with rub: (a) $p = 1/5$, (b) $p = 1/3$, and (c) $p = 1/2$.

5. Experimental results

The experimental work is carried out on a rotor-bearing system that consists of a circular steel shaft with central disk supported on a pair of ball bearings (Fig. 15). An induction motor drives the system through three

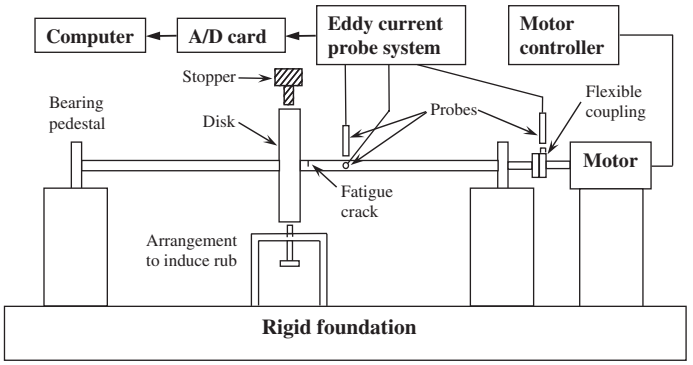

Fig. 15. Schematic of experiment setup.

jaw flexible coupling. The alignment between motor shaft and rotor shaft is done using reverse dial indicator method. Provision is made to induce rub in the system using an arrangement shown in Fig. 15. Stopper is also provided above the disk, to limit higher vibration levels, which otherwise may damage the sensors.

Since, the study covers vibration response of uncracked and cracked rotor with and without rub, two shafts; one uncracked and other cracked are used in experiments. A transverse fatigue crack is developed using three-point fatigue bending method on a fatigue tester. To initiate the fatigue crack at desired location, a fine slit of about 0.7–1.0 mm depth is made using jeweller's saw. The shaft is placed on a fatigue-bending machine and subjected to cyclic loading, until the crack is propagated to a desired depth. Cracked shaft with crack depth ratio of $a/D = 0.28$, is used for present work. The crack is located at 3 mm from the disk face. Disk weighs 5.65 kg. Both the shafts, i.e. uncracked and cracked, have 25 mm diameter and 0.7 m length between bearings. Single row deep groove ball bearings (SKF 6204) are used to support the rotor. The rotor is driven using Siemens make 750W-3 phase induction motor with Micromaster controller.

Vibrations are sensed using Bently Nevada make eddy current proximity probes (3300 series). The eddy current probes sense the vibration signals of the rotating shaft. Two probes are used to monitor vibrations in horizontal and vertical directions. One additional probe is kept near the coupling, signal from it act as the reference signal. Vibrations sensed by the probes are conditioned by proximeter before sending it to A/D card plugged to the computer. A Labview^{TM} program is written to acquire the vibration data using A/D card. The digitized data are stored, which can be processed further to extract useful diagnostic information.

Experiments are carried out for uncracked and cracked rotors with and without rub. The bending natural frequency of the rotors is found to be 48 Hz. The electric motor is operated at constant subcritical speeds, $p = 1/3$ and $1/2$ (i.e. 16 and 24 Hz, respectively). These speeds correspond to the integer fraction of bending critical speed of the rotor, which are found using rap test on the rotors. The steady-state lateral vibration signals are recorded using probes i.e. horizontal and vertical directions and results are presented in the form of full spectrum plots. Whenever required, rub is induced at disk location by adjusting the gap between disk and bolt. The bolt is advanced to a desired position until rub impact is observed. Finally, locknut is tightened to restrict further movement of the bolt. Experimental results are first discussed for rotors without rub and then with rub.

Fig. 16 shows the full spectrum plots of the vibration response of uncracked rotor with residual unbalance. Forward whirling 1X component dominates the spectra. Weak harmonics i.e. 2X, 3X, etc. are also present, however, at $p = 1/2$, 2X increases to a noticeable magnitude. Appearance of harmonics in a rotor system, where unbalance is the only known rotor fault, is due to residual misalignment and other inherent nonlinearity of the rotor-bearing system. Vertical vibration signals and full spectra of the cracked rotor are presented in Fig. 17. There is an increase in magnitude of 1X, 2X, and 3X harmonics in comparison with the uncracked rotor. Furthermore, these harmonics exhibit forward whirl. When $p = 1/3$, -3X component of considerable magnitude appears where as at $p = 1/2$, -2X is relatively very weak compared with $+2$X harmonics. This is a clear experimental validation of strong forward whirl nature of 2X vibration for cracked rotor as observed through numerical study (Fig. 9). Forward whirling nature of the unbalance and crack ($a/D = 0.28$)

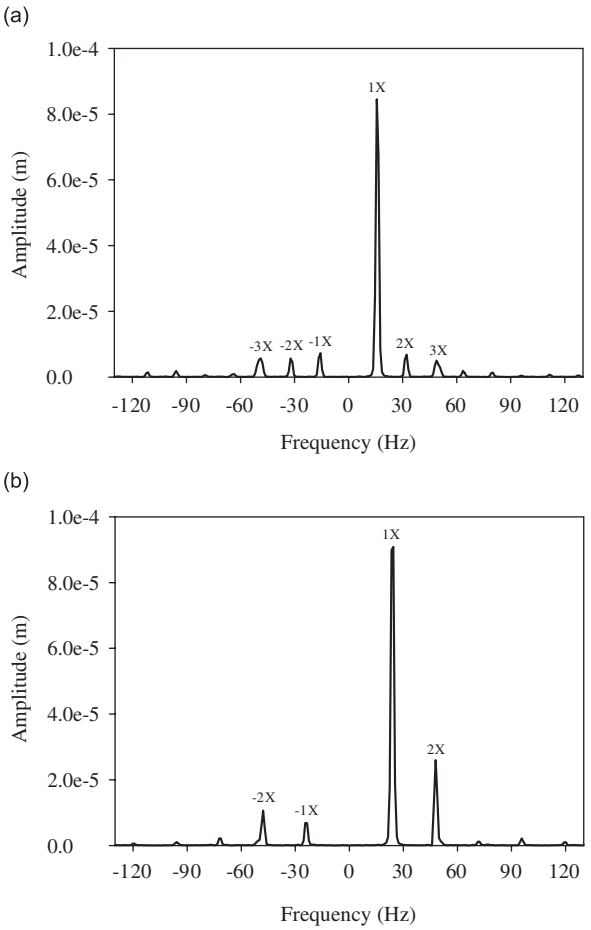

Fig. 16. Full spectra of experimental response of uncracked rotor without rub: (a) $p = 1/3$ and (b) $p = 1/2$.

excitations, found in numerical simulations (Figs. 5 and 9) are also verified from experimental investigations (Figs. 16 and 17).

The experimental response of rub in uncracked rotor is shown in Fig. 18. Rub generates many harmonics in the spectrum, particularly when $p = 1/3$. For $p = 1/2$, first three harmonics are significant. Nevertheless, 1X frequency still dominates the spectra. The higher harmonics appear on both sides of the full spectrum (i.e. along +ve and −ve frequency axis). This feature is typical to a rotor rub and should be used for rub diagnosis. From the full spectrum plots, most of the higher harmonics appear to be the same in magnitude along both sides of the spectrum. However, the numerical values of +ve and −ve frequency components listed in Table 1 for the first five harmonics point out that the vibration motion at these harmonics is forward whirling. Subharmonic resonances are not observed in this case. It may be noticed that the vibration waveforms of the cracked rotor without rub (Fig. 17(a) and (c)) and rub in uncracked rotor (Fig. 18(a) and (c)) look quite similar and hence may not directly and conclusively point out the type of malfunctions prevailing in the system. However, their full spectra are quite distinct and could indicate the developing rotor fault. Full spectra of the cracked rotor (Fig. 17(b) and (d)) is dominated by forward whirling first three harmonics, however, full spectra for rub in uncracked rotor (Fig. 18(b) and (d)) show spectrum rich in harmonics (up to sixth harmonic) with almost equal forward and backward whirl components. Fig. 19 shows the vibration waveforms and full spectra for rub in cracked rotor case. Vibrations at 2X frequency component are backward whirling for both the speeds, i.e. $p = 1/2$ and $1/3$. Response at 3X is clearly backward whirling for $p = 1/3$, which is its corresponding subharmonic resonance speed. When $p = 1/2$, 3X harmonic reduces and is of negligible value.

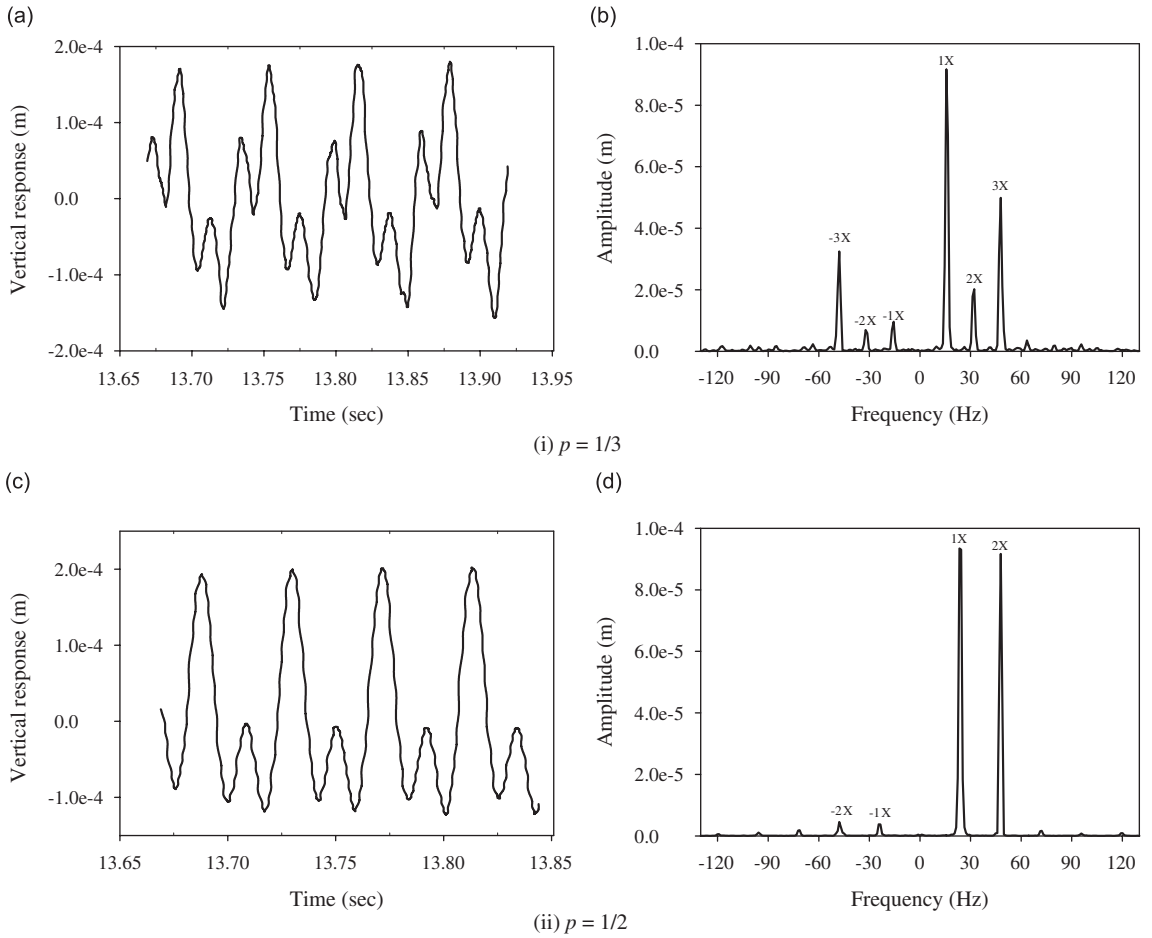

Fig. 17. Vibration response and full spectrum plots of experimental response of cracked rotor without rub: (a, c) vertical vibration response; (b, d) full spectra; (i) $p = 1/3$ and (ii) $p = 1/2$.

It may be noted that for uncracked rotor with rub, 3X was significant in the spectra at $p = 1/2$. Table 2 lists the amplitude of $+$ve and $-$ve frequency components.

Experimental observations for rub in uncracked and cracked rotors are corroborating the numerical findings. It is important to note that, for the case of rub in uncracked rotor, the difference between forward and backward spectral components is too small for most of the times and may not be distinguished from experimental vibration signals. Hence, establishing the exact directional nature for such harmonics is difficult. However, for rub in cracked rotor, difference in forward and reverse 2X and 3X harmonics is of significant magnitude and can be used with confidence to establish the whirl nature of the vibrations at these harmonics. From the numerical and experimental investigations presented for rotor speeds at integer submultiples of natural frequency, the salient observations regarding the whirl nature of the rotor faults (i.e. crack, rub and rub with crack) is tabulated in Table 3.

It should be noted that the results presented here are for a rotor system having fatigue crack near center of the rotor span. The rotor stator rub is considered between disk and stator at the disk location, which is also situated centrally on the shaft span. Locations of crack and rub are close to each other; at the center of the shaft span. The results are applicable to the case when crack and rub are close to each other and in the mid-span. The main focus in the paper was to consider these two important faults in the rotor-bearing system together and understand the effects of them being simultaneously present. Since Jeffcott rotor model has been considered for simplicity, it was not possible to investigate relative influence of spacing between crack, rub and sensor locations on the results presented in this study. Indeed it would be interesting to understand to what

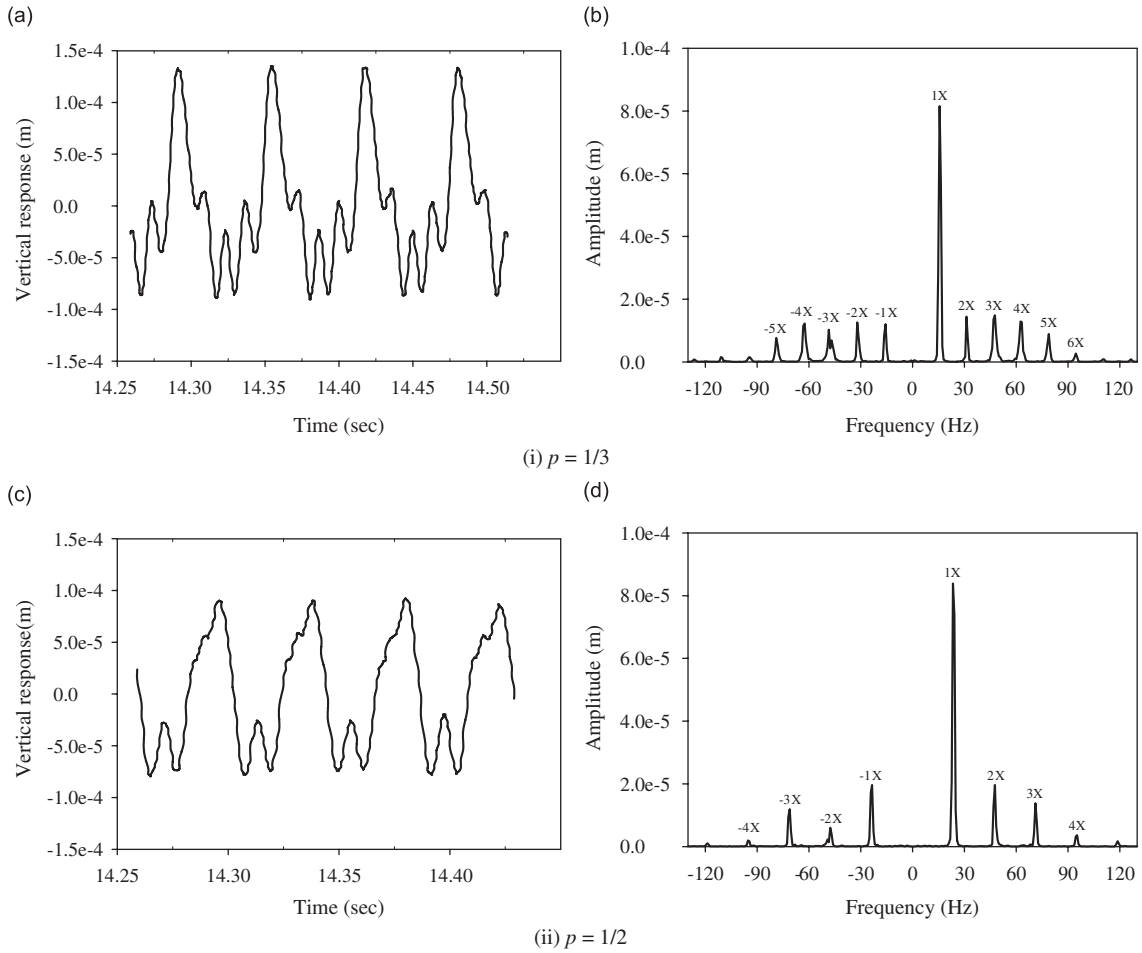

Fig. 18. Vibration response and full spectrum plots of experimental response of uncracked rotor with rub: (a, c) vertical vibration response; (b, d) full spectra; (i) $p = 1/3$ and (ii) $p = 1/2$.

Table 1
Spectral components for rub in uncracked rotor

Speed ratio	Frequency order	Positive (+ve) frequency amplitude (m)	Negative (−ve) frequency amplitude (m)	Whirl nature
$p = 1/3$	1X	8.155e−05	1.203e−05	Forward
	2X	1.443e−05	1.254e−05	Forward
	3X	1.488e−05	1.027e−05	Forward
	4X	1.268e−05	1.224e−05	Forward
	5X	0.888e−05	0.761e−05	Forward
$p = 1/2$	1X	8.384e−05	1.965e−05	Forward
	2X	1.962e−05	0.600e−05	Forward
	3X	1.381e−05	1.194e−05	Forward
	4X	0.363e−05	0.196e−05	Forward
	5X	0.170e−05	0.104e−05	Forward

extent this factor (i.e. location of crack, rub, and sensors) plays role in the observed dynamic phenomenon. For this purpose, the current model of rotor system would be extended to finite element approach in future study. However, the maximum displacement and likelihood of rotor–stator contact is more in the mid-span in

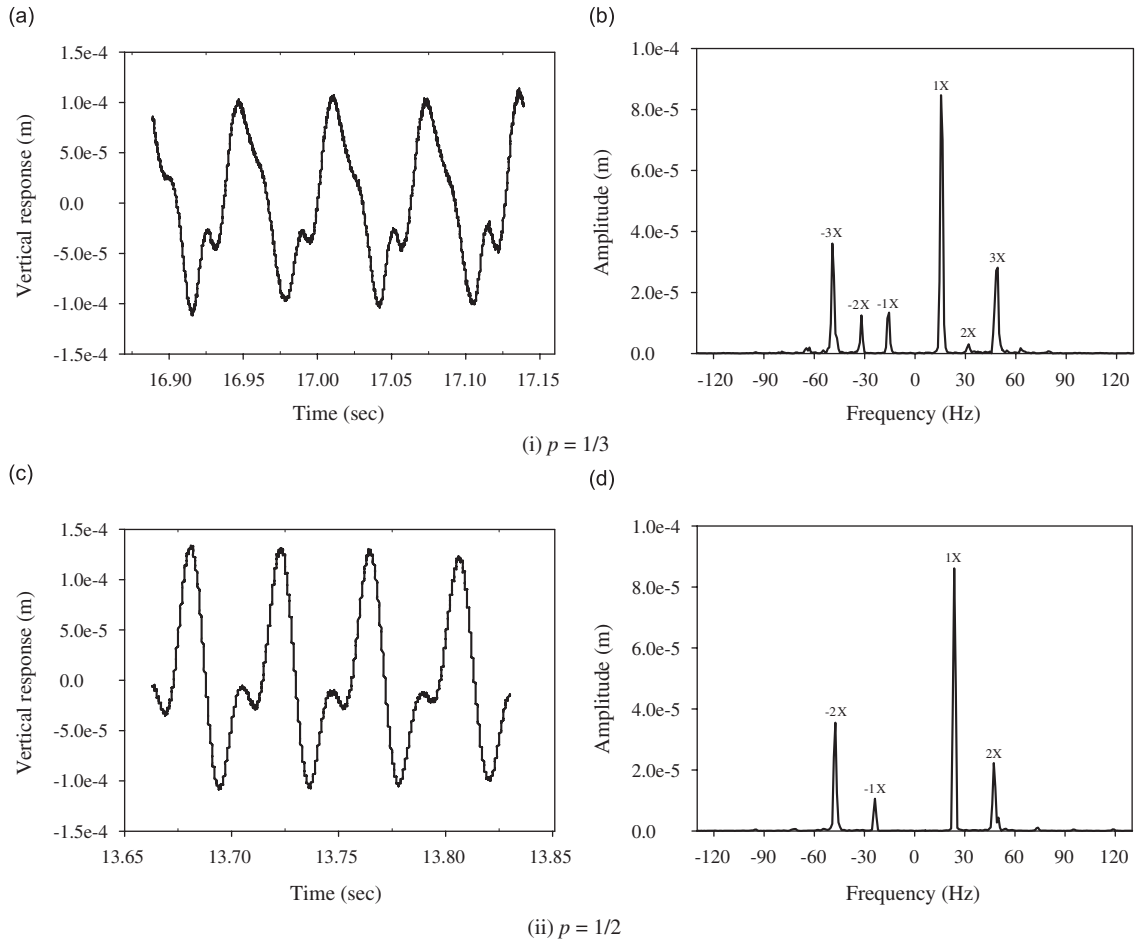

Fig. 19. Vibration response and full spectrum plots of experimental response of cracked rotor with rub: (a, c) vertical vibration response; (b, d) full spectra; (i) $p = 1/3$ and (ii) $p = 1/2$.

Table 2
Spectral components for rub in cracked rotor

Speed ratio	Frequency order	Positive (+ve) frequency amplitude (m)	Negative (−ve) frequency amplitude (m)	Whirl nature
$p = 1/3$	1X	8.466e−05	1.343e−05	Forward
	2X	0.300e−05	1.256e−05	Backward
	3X	2.815e−05	3.601e−05	Backward
	4X	0.176e−05	0.194e−05	Forward
	5X	0.072e−05	0.064e−05	Forward
$p = 1/2$	1X	8.609e−05	1.051e−05	Forward
	2X	2.224 e−05	3.546e−05	Backward
	3X	0.110e−05	0.064e−05	Forward
	4X	0.048e−05	0.046e−05	Forward
	5X	0.054e−05	0.004e−05	Forward

a normal speed range of operation of rotor. Similarly, due to the fact that likely chances of rotor crack is also near the center of the shaft for similar reasons and larger bending stress, the location of crack and rub considered in the present study caters to the most likely situation.

Table 3
Whirl nature of rotor vibration response for different faults

Frequency order	Cracked rotor	Rotor rub	Rub in cracked rotor
1X	Forward whirling with weak −1X component	Forward whirling with significant −1X component	Forward whirling with significant −1X component
2X	Strongly forward whirling with negligible −2X	+2X and −2X are mostly equal in magnitude	Strong +2X and −2X components with backward whirling vibration motion
3X and 5X at $p = 1/3, 1/5$, respectively	Forward whirling with weak −3X and −5X	Positive (+ve) and −ve frequency components are almost equal	Backward whirling

6. Conclusions

Common practice for fault identification in a rotor system is to look for individual fault symptoms in the vibration response. However, a typical rotor system is likely to have more than one fault present in the system. This paper presents one such case, where multiple faults are considered together in a rotor system, i.e. unbalance, crack, and rub. Numerical simulations and experimentations are carried out and vibration signals are analyzed using full spectrum analysis. It is revealed that the relative phase information between the vibration signals in two directions is important to relate the nature of vibration excitations with the rotor faults. The present study shows that full spectrum utilizes this directivity information of the rotor orbit and effectively reveals the whirl nature of the excitation frequencies. It has been shown that experimental investigations matches well with the theoretical findings. From the investigations, relatively new diagnostic recommendations are proposed, when rub occurs in the cracked rotor.

Excitations due to unbalance and crack are strongly forward whirling in nature. Vibration motion at 2X harmonic is strongly forward in cracked rotor, in comparison with vibrations at 1X, 3X, and 5X harmonics. Since rub-impact is transient in nature, it gives broadband excitation and the spectrum of the rub signals shows numerous spectral lines. It has been shown that rub in uncracked rotor excites forward and backward whirl frequencies almost equally and this is suggested as fault feature typical of rotor rub. When the rub is to be identified in the cracked rotors, it is important to observer the nature of the 2X vibration motion. It has been shown that when rub develops in the cracked rotor, the original strong forward 2X vibration motion of the cracked rotor (typical of crack fault) changes to backward whirling. This trend is observed for all rotational speeds up to half the bending critical speed. Backward whirl nature of higher harmonics at corresponding subharmonic resonances i.e. backward whirl nature of 5X at $p = 1/5$ and that of 3X at $p = 1/3$ is also recommended to identify rub in a cracked rotor.

References

[1] A.D. Dimarogonas, Vibration of cracked structures: a state of art review, *Engineering Fracture Mechanics* 55 (1996) 831–857.
[2] G. Sabnavis, R.G. Kirk, M. Kasarda, D. Quinn, Cracked shaft detection and diagnostics: a literature review, *The Shock and Vibration Digest* 36 (2004) 287–296.
[3] O.S. Jun, H.J. Eun, Y.Y. Earmme, C.W. Lee, Modelling and vibration analysis of a simple rotor with breathing crack, *Journal of Sound and Vibration* 155 (1992) 273–290.
[4] J.J. Sinou, A.W. Lees, The influence of cracks in rotating shafts, *Journal of Sound and Vibration* 285 (2005) 1015–1037.
[5] T. Zhou, Z. Sun, J. Xu, W. Han, Experimental analysis of cracked rotor, *Journal of Dynamical Systems, Measurements, and Control* 127 (2005) 313–320.
[6] A. Muszynska, *Rotordynamics*, CRC Press, Boca Raton, FL, Taylor & Francis, London, 2005.
[7] R.F. Beatty, Differentiating rotor response due to radial rubbing, *Journal of Vibration Acoustics, Stress and Reliability in Design* 107 (1985) 151–160.
[8] F. Ehrich, High-order subharmonic response of high speed rotors in bearing clearance, *Journal of Vibration Acoustics, Stress and Reliability in Design* 110 (1988) 9–16.

[9] Z. Feng, X. Zhang, Rubbing phenomena in rotor–stator contact, *Chaos, Solutions and Fractals* 14 (2002) 257–267.
[10] F. Chu, W. Lu, Experimental observation of nonlinear vibrations in a rub-impact rotor system, *Journal of Sound and Vibration* 283 (2005) 621–643.
[11] N. Bachschmid, P. Pennacchi, A. Vania, Identification of multiple faults in rotor systems, *Journal of Sound and Vibration* 254 (2002) 327–366.
[12] R.K. Chan, T.C. Lai, Digital simulation of a rotating shaft with a transverse crack, *Applied Mathematical Modelling* 19 (1995) 411–420.
[13] A.K. Darpe, K. Gupta, A. Chawla, Dynamics of a two-cracked rotor, *Journal of Sound and Vibration* 259 (2003) 649–675.
[14] A.K. Darpe, K. Gupta, A. Chawla, Dynamics of a bowed rotor with a transverse surface crack, *Journal of Sound and Vibration* 296 (2006) 888–907.
[15] F. Wan, Q. Xu, S. Li, Vibration analysis of cracked rotor sliding bearing system with rotor–stator rubbing by harmonic wavelet transform, *Journal of Sound and Vibration* 271 (2004) 507–518.
[16] P. Goldman, A. Muszynska, Application of full spectrum to rotating machinery diagnostics, *Orbit First Quarter* (1999) 17–21.
[17] C.W. Lee, Y.S. Han, The directional Wigner distribution and its application, *Journal of Sound and Vibration* 216 (1998) 585–600.
[18] N. Bachschmid, P. Pennacchi, A. Vania, Diagnostic significance of orbit shape analysis and its application to improve machine fault detection, *Journal of Brazilian Society of Mechanical Sciences and Engineering* 26 (2004) 200–208.
[19] W. Fengqi, G. Meng, Compound rub malfunctions feature extraction based on full spectrum cascade analysis and SVM, *Mechanical Systems and Signal Processing* 20 (2006) 2007–2021.
[20] H. Tada, P.C. Paris, G.R. Irwin, *The Stress Analysis of Cracks Handbook*, Del Research Corporation, Hellertown, Pennsylvania, 1973.
[21] W. Mayes, W.G.R. Davis, The vibration behaviour of a multi-shaft, multi-bearing system in the presence of a propagating transverse crack in a rotor, *Journal of Vibration, Acoustics, Stress and Reliability in Design* 106 (1984) 146–153.